Calculation of pair production by 10 and 20 MeV photons

L. E. Wright, K. K. Sud,* and D. W. Kosik
Department of Physics and Astronomy, Ohio University, Athens, Ohio 45701
(Received 23 March 1987)

We present new techniques for calculating electron-positron pair production in the field of a fixed point charge in distorted-wave Born approximation which permits the evaluation of the Dirac-Coulomb radial matrix elements for lepton energies much greater than the electron rest mass, and for large angular momenta. Using these techniques, the pair production cross sections for 10 and 20 MeV photons on uranium ($Z=92$) are evaluated and compared to the so-called "bridging formulae" which connect the low energy ($\omega < 5$ MeV) distorted-wave Born approximation results to the approximate results for high energy ($\omega > 50$ MeV) obtained with the Sommerfeld-Maue approximation and to the experimental results.

I. INTRODUCTION

Total photon absorption cross section measurements have been carried out by a number of workers[1-4] in the intermediate energy range. The aim of these measurements has been to extract the photonuclear cross section. The nuclear absorption cross section is the difference between the total absorption cross section σ_t and the atomic cross section σ_a which results from the electromagnetic interaction of photons with an atom and includes the photoelectric effect, pair production, triplet production, and the Compton effect. That is,

$$\sigma_{\text{nuc}}=\sigma_t-\sigma_a \ . \tag{1}$$

The nuclear absorption cross section is at most 5% of the total absorption cross section in the intermediate energy range ($\omega=5-50$ MeV). Therefore, it is essential to know the atomic cross sections as well as the total absorption cross section as accurately as possible in order to extract the nuclear absorption cross section. For details of the present status of total photon absorption cross section measurements and theoretical calculations of the atomic cross sections, we refer the reader to the recent tabulations of Gimm and Hubbell[5] and Hubbell *et al.*[6] In the intermediate energy range the atomic absorption is dominated by the pair production process. For lead, e.g., 74% at 10 MeV and 87% at 20 MeV of the total cross section is due to pair production in the field of the atomic nucleus. Therefore, there is considerable interest in the theoretical evaluation of the pair production cross section.

Bethe and Heitler[7] have calculated the pair production cross section in the Coulomb field of the nucleus in the plane wave (PW) approximation. However, this approximation is not valid for high Z elements or for low Z elements in the low energy region and, therefore, one needs "Coulomb corrections" to the PW calculation. This means that the leptons can no longer be represented by Dirac plane waves.

For a more exact calculation, one includes the effects of the static Coulomb field in the lepton wave functions by including the Coulomb potential in the Dirac equation. With the use of Dirac-Coulomb waves, pair production occurs in first order and keeping only the first order term is referred to as the distorted wave Born approximation (DWBA). A number of DWBA calculations for the pair production in the low energy region are available in the literature.[8-11] In particular, Overbo *et al.*[9] have carried DWBA calculations from threshold to photon energies of 5 MeV where their techniques break down. The DWBA calculation for a fixed electron energy in the tip region of the positron spectrum in the energy range 5–10 MeV is also available.[12] At high energies (photon energy $\omega > 50$ MeV), the calculation of Davies, Bethe, and Maximon[13] (DBM) using the Sommerfeld-Maue approximation for the lepton wave functions should be accurate. Recently, there have been attempts to construct semiempirical bridging formulae by Overbo[14] and Maximon and Gimm[15] by choosing a reasonable analytic function of Z and ω along with a number of parameters such that the formula approaches the DBM result in the high energy limit. The parameters are fitted to the low energy results of Overbo *et al.*[9] However, the two reasonable analytic functions are different and the two different bridging formulae give different results in the intermediate energy region.[15] Thus there exists an energy range from 5 to 50 MeV or more where the Coulomb distortion correction to the Bethe-Heitler result is reasonably large and uncertain for medium and heavy nuclei. The Coulomb distortion effect remains the single largest uncertainty in the extraction of the photonuclear cross section from total photon absorption measurements.[15]

In this paper we apply some recently developed mathematical techniques for evaluating the Dirac-Coulomb radial matrix elements for the process of pair production from a fixed point charge in order to evaluate the Coulomb distortion effects in the intermediate energy region.[12,16-22] In Sec. II we give the DWBA formulas for pair production along with our technique for evaluating the radial integrals. In Sec. III we outline the calculational details and in Sec. IV we give our results for 10 and 20 MeV photons on uranium ($Z=92$). We compare these results to the bridging formulae and to the experimental results of Sherman *et al.*[3] Due to the large amount of computer time required for these calculations, we have not yet

evaluated the pair production cross section at other energies nor for other nuclei. However, the Coulomb distortion changes rapidly in the energy region from 5 to 20 MeV, so that our values for the most distorting nucleus should provide a good test of the bridging formulae as well as testing the assumptions made in extracting experimental pair production cross sections from the total photon absorption measurements.

II. PAIR PRODUCTION IN THE DWBA

In a distorted wave calculation, the Coulomb distortion arising from the spherically symmetric static charge distribution of the atomic nucleus is included exactly by solving the Dirac equation for leptons in the presence of the associated potential. By using these states as basis states (Dirac-Coulomb wave functions) and treating the time dependent part of the interaction to first order, we perform a distorted wave Born approximation analysis. Since in DWBA the Coulomb potential acts continuously, it is equivalent to summing all plane wave Feynman diagrams for the spherically symmetric part of the static Coulomb field. We represent the Dirac-Coulomb waves diagrammatically by curved lines in the DWBA diagram for pair production shown in Fig. 1. In the following subsection we give the lepton Dirac-Coulomb wave functions needed for subsequent discussion.

A. Dirac-Coulomb wave functions

The Dirac equation for a central potential $V=V(r)$ can only be separated in spherical coordinates, and thus the Dirac-Coulomb wave functions are a superposition of spherical wave solutions. For an electron with spin m_s, energy E, mass m, and momentum p, the Dirac-Coulomb wave function in the point Coulomb field of a charge Ze is

$$\psi_{\pm}^{m_s}(\mathbf{r})=4\pi\left[\frac{E+m}{2E\mathcal{V}}\right]^{1/2}\sum_{\kappa,\mu}e^{\pm i\delta_\kappa}i^l C_{\mu-m_s\ m_s\ \mu}^{\ l\ \ 1/2\ \ j}\times Y_l^{\mu-m_s*}(\hat{\mathbf{p}})\psi_\kappa^\mu(\mathbf{r}) , \quad (2)$$

where $+$ (or $-$) denotes outgoing (or incoming) spherical waves and $\mathcal{V}$ is the normalization volume. The spinor $\psi_\kappa^\mu(\mathbf{r})$ is given as

$$\psi_\kappa^\mu(\mathbf{r})=\begin{bmatrix} g_\kappa(r) & \chi_\kappa^\mu(\hat{\mathbf{r}}) \\ if_\kappa(r) & \chi_{-\kappa}^\mu(\hat{\mathbf{r}})\end{bmatrix} , \quad (3)$$

where κ is the Dirac quantum number which determines the orbital angular momentum l and the total angular momentum j by $j=|\kappa|-\frac{1}{2}$ and $l=|\kappa+\frac{1}{2}|-\frac{1}{2}$. The spin-angle functions are given in terms of the Pauli spinor

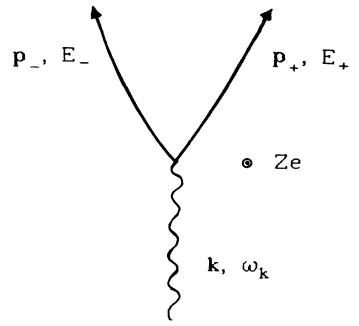

FIG. 1. Pair production in the DWBA.

by

$$\chi_\kappa^\mu(\hat{\mathbf{r}})=\sum_\nu C_{\mu-\nu\ \nu\ \mu}^{\ l\ \ 1/2\ \ j}Y^{\mu-\nu}(\hat{\mathbf{r}})\chi^\nu , \quad (4)$$

and the radial functions $f_\kappa(r)$ and $g_\kappa(r)$ are real and obey the first-order matrix differential equation

$$\frac{dU(r)}{dr}=\left[\frac{A}{r}-B\right]U(r) , \quad (5)$$

where

$$U(r)=\begin{bmatrix} r\ g_\kappa(r) \\ r\ f_\kappa(r)\end{bmatrix} ,$$
$$A=\begin{bmatrix} -\kappa & \alpha Z \\ -\alpha Z & \kappa\end{bmatrix} , \quad (6)$$
$$B=\begin{bmatrix} 0 & -(E+m) \\ E-m & 0\end{bmatrix} .$$

The phase factor in Eq. (2) is given by

$$\delta_\kappa=\eta_c-\gamma\frac{\pi}{2}+\frac{\pi}{2}(l+1)-\arg[\Gamma(\gamma+i\eta)] , \quad (7)$$

where

$$\eta_c=-\frac{\pi}{2}\left[\frac{\kappa+|\kappa|}{2|\kappa|}\right]-\tfrac{1}{2}\tan^{-1}\left[\frac{\eta(\kappa+m\gamma/E)}{\kappa\gamma-m\eta^2/E}\right]$$

and

$$\gamma=(\kappa^2-\alpha^2Z^2)^{1/2},\quad \eta=\alpha ZE/p .$$

In Eq. (7), Γ is the conventional gamma function and the principal value of $\tan^{-1}$ is to be taken. The Dirac-Coulomb functions (DC) are given explicitly in terms of the confluent hypergeometric functions by

$$\begin{bmatrix} g_\kappa(r) \\ f_\kappa(r)\end{bmatrix}=\begin{bmatrix} 1 \\ -p/(E+m)\end{bmatrix}\frac{(2pr)^\gamma e^{\pi\eta/2}}{pr\Gamma(2\gamma+1)}\,|\Gamma(\gamma+i\eta)|\begin{bmatrix}\mathrm{Re} \\ \mathrm{Im}\end{bmatrix}(\gamma+i\eta)e^{i\eta_c}e^{-ipr}\,{}_1F_1(\gamma+1+i\eta,\,2\gamma+1;\,2ipr) .$$

Distorted wave functions for electrons will be denoted by using a minus subscript on various parameters in Eqs. (2)–(9) e.g., E_- (energy), $\mathbf{p}_-$ (momentum), $U_-(r)$, A_-, B_-, etc. For positron scattering in the same Coulomb field of the nucleus, the distorted wave functions with a plus subscript are obtained by making the replacements $E_-=-E_+$ and $\mathbf{p}_-=-\mathbf{p}_+$ everywhere.

As noted in the Introduction, the Sommerfeld-Maue

approximation has been used to calculate pair production at higher photon energies. The Sommerfeld-Maue wave function (SM) corresponds to an approximate solution of the Dirac equation is closed form, and can be written for an electron of spin m_s,

$$\phi_{\rm SM}^{m_s}=\phi_0^{m_s}+\phi_1^{m_s} =Ne^{i\mathbf{p}\cdot\mathbf{r}}\left[1-\frac{i}{2E}\boldsymbol{\alpha}\cdot\boldsymbol{\nabla}\right]{}_1F_1[i\eta,\,1;\,i(pr-\mathbf{p}\cdot\mathbf{r})]u^{m_s}(\mathbf{p}) , \tag{8}$$

where $u^{m_s}(\mathbf{p})$ is the plane wave Dirac spinor and the normalization $N=\Gamma(1-i\eta)e^{\pi\eta/2}/\sqrt{\mathcal{V}}$. Johnson and Deck[23] have investigated the relationship between the SM and DC wave functions, and upon making a partial wave expansion of both find that for $\gamma\rightarrow\kappa$ the distorted wave function $\psi_{\pm}^{m_s}$ defined in Eq. (2) reduces to the Sommerfeld-Maue wave function defined in Eq. (8). That is,

$$\lim_{\gamma\rightarrow|\kappa|}\psi_{\pm}^{m_s}=\phi_{\pm}^{m_s} . \tag{9}$$

In other words, the Sommerfeld-Maue wave function is a good approximation to the Dirac-Coulomb wave function for large angular momentum since $\gamma=|\kappa|(1-\alpha^2Z^2/2|\kappa|^2+\ldots)$. This result will be used in Sec. III to assist in performing the angular momentum sums and the details of the relationship between the SM and DC functions is extensively discussed in Ref. 20.

B. Scattering amplitude and cross section

The Hamiltonian density for leptons and photons in a static electromagnetic field is

$$H=H_{\rm rad}+H_{\rm DC}+H_{\rm int} , \tag{10}$$

where the Hamiltonian for the electromagnetic field in free space in second quantized form can be written as

$$H_{\rm rad}=\sum_{k,\lambda}(a_{\mathbf{k},\lambda}^{\dagger}a_{\mathbf{k},\lambda}+\tfrac{1}{2}) . \tag{11}$$

In the radiation gauge this corresponds to the potentials

$$\phi(\mathbf{r},t)=0 ,$$
$$\mathbf{A}(\mathbf{r},t)=\sum_{k,\lambda}\left[\frac{2\pi}{\omega_k}\right]^{1/2}\{a_{\mathbf{k},\lambda}\mathbf{u}_{\mathbf{k},\lambda}(\mathbf{r})e^{-i\omega_k t}+a_{\mathbf{k},\lambda}^{\dagger}u_{\mathbf{k},\lambda}^{*}e^{i\omega_k t}\} , \tag{12}$$

where

$$\mathbf{u}_{\mathbf{k},\lambda}=\left[\frac{1}{\mathcal{V}}\right]^{1/2}\hat{\boldsymbol{\epsilon}}_{\lambda}e^{i\mathbf{k}\cdot\mathbf{r}} ,$$

and λ denotes the polarization state of photons propagating with momentum $\mathbf{k}$ and $\mathcal{V}$ is the normalization volume. The Dirac-Coulomb Hamiltonian for a lepton in the spherically symmetric static Coulomb potential of the nucleus is given as

$$H_{\rm DC}=-i\boldsymbol{\alpha}\cdot\boldsymbol{\nabla}+V(r)+m\beta , \tag{13}$$

where $\boldsymbol{\alpha}$ and β are standard Dirac matrices and $V(r)=\mp\alpha Z/r$ for electrons $(-)$ and positrons $(+)$, respectively. The interaction Hamiltonian for an electron (or a positron) in an electromagnetic field is described by the scalar and vector potential ϕ and $\mathbf{A}$ as

$$H_{\rm int}=q[\phi(\mathbf{r},t)-\boldsymbol{\alpha}\cdot\mathbf{A}(\mathbf{r},t)] , \tag{14}$$

where $q=\mp e$.

In the radiation gauge the interaction Hamiltonian reduces to $H_{\rm int}=-q\boldsymbol{\alpha}\cdot\mathbf{A}(\mathbf{r},t)$. The scattering amplitude for pair production is obtained by using the eigenstates of $H_{\rm rad}+H_{\rm DC}$ as basis states and treating $H_{\rm int}$ by first order perturbation theory. A photon of energy ω, momentum $\mathbf{k}$, and polarization $\hat{\boldsymbol{\epsilon}}_{\lambda}$, while passing through the Coulomb field of an infinitely heavy nucleus of charge Ze, is absorbed by an electron of negative energy $-E_+$, momentum $-\mathbf{p}_+$, and spin m_+, which makes a transition to an electron of positive energy E_-, momentum $\mathbf{p}_-$, and spin m_-. The explicit expression for the amplitude is given as

$$a_{fi}=-2\pi i\delta(E_++E_--\omega)V_{f,i} , \tag{15}$$

where

$$V_{f,i}=-e\left[\frac{2\pi}{\omega\mathcal{V}}\right]^{1/2}\int_{\mathcal{V}}\psi_-^{m_-\dagger}\boldsymbol{\alpha}\cdot\hat{\boldsymbol{\epsilon}}_{\lambda}e^{i\mathbf{k}\cdot\mathbf{r}}\psi_+^{m_+}d^3r . \tag{16}$$

In order to perform the angular integrals in Eq. (16), we expand the photon field into multipoles,

$$\hat{\boldsymbol{\epsilon}}_{\lambda}e^{i\mathbf{k}\cdot\mathbf{r}}=\lambda(2\pi)^{1/2}\sum_{L,M}\sqrt{(2L+1)}i^LD_{M\lambda}^{L}(\hat{\mathbf{k}}) \times[\mathbf{A}_{LM}^{(m)}(\mathbf{r})+i\lambda\mathbf{A}_{LM}^{(e)}(\mathbf{r})] , \tag{17}$$

where $\hat{\boldsymbol{\epsilon}}_{\lambda}$ is in the spherical basis and $D_{M,\lambda}^{L}(\hat{\mathbf{k}})$ are rotation matrices. The transverse electric and magnetic vector multipole potentials are

$$\mathbf{A}_{L,M}^{(m)}(\mathbf{r})=j_L(kr)\mathbf{Y}_{L,L}^{M}(\hat{\mathbf{r}}) ,$$
$$\mathbf{A}_{L,M}^{(e)}(r)=\left[\frac{L+1}{2L+1}\right]^{1/2}j_{L-1}(kr)\mathbf{Y}_{L,L-1}^{M}(\hat{\mathbf{r}}) -\left[\frac{L}{2L+1}\right]^{1/2}j_{L+1}(kr)\mathbf{Y}_{L,L+1}^{M}(\hat{\mathbf{r}}) . \tag{18}$$

We choose $\mathbf{k}=k\hat{\mathbf{z}}$, and using $D_{M,\lambda}^{L}(\hat{\mathbf{z}})=\delta_{M,\lambda}$ the expansion in Eq. (17) can be expressed as

$$\hat{\boldsymbol{\epsilon}}_{\lambda}e^{i\mathbf{k}\cdot\mathbf{r}}=\sqrt{2\pi}\lambda\sum_{L}\sqrt{2L+1}i^L[\mathbf{A}_{L,\lambda}^{(m)}(\mathbf{r})+i\lambda A_{L,\lambda}^{(e)}(\mathbf{r})] . \tag{19}$$

Substituting the multipole expansion in Eq. (19) and the partial wave expansion for electron and positron wave functions given in Eq. (2) into Eq. (16), and carrying out the angular integrals, we obtain

$$V_{f,i}=-e(4\pi)^3\lambda\left[\frac{(E_++m)(E_-+m)}{4E_+E_-\omega\mathcal{V}^3}\right]^{1/2}\sum_{\substack{\kappa_+,\kappa_-\\ \mu_+,\mu_-,L}}\left[\frac{(2L+1)(2j_++1)}{16\pi}\right]^{1/2}e^{i(\delta_{\kappa_+}+\delta_{\kappa_-})}i^{(l_+-l_-+L-1)}$$

$$\times C^{l_-}_{\mu_--m_-}{}^{1/2}_{m_-}{}^{j_-}_{\mu_-}C^{l_+}_{\mu_+-\mu_+}{}^{1/2}_{m_+}{}^{j_+}_{\mu_+}C^{j_+}_{-1/2}{}^{j_-}_{1/2}{}^{L}_{0}C^{j_+}_{\mu_+}{}^{L}_{\lambda}{}^{j_-}_{\mu_-}R(\kappa_+,\kappa_-,L\lambda)Y^{\mu_--m_-}_{l_-}(\hat{\mathbf{p}}_-)Y^{\mu_+-m_-*}_{l_+}(-\hat{\mathbf{p}}_+)\ , \tag{20}$$

where the radial integral R is given as

$$R(\kappa_+,\kappa_-,L\lambda)=S_{l_+,\bar{l}_-,L}I^{(m)}(\kappa_+,\kappa_-,L)+i\lambda S_{l_+,l_-,L}I^{(e)}(\kappa_+,\kappa_-,L)\ . \tag{21}$$

and $\bar{l}(\kappa)=l(-\kappa)$. The magnetic multipole radial integral $I^{(m)}$ and electric multipole radial integral $I^{(e)}$ are given by

$$I^{(m)}=\frac{\kappa_++\kappa_-}{\sqrt{L(L+1)}}\int_0^\infty j_L(\omega r)(f_{\kappa_-}g_{\kappa_+}+g_{\kappa_-}f_{\kappa_+})r^2dr\ , \tag{22}$$

$$I^{(e)}=-\frac{\sqrt{L(L+1)}}{2L+1}\int_0^\infty\left\{j_{L-1}\left[(f_{\kappa_-}g_{\kappa_+}-g_{\kappa_-}f_{\kappa_+})-\frac{\kappa_+-\kappa_-}{L}(f_{\kappa_-}g_{\kappa_+}+g_{\kappa_-}f_{\kappa_+})\right]\right.$$
$$\left.+j_{L+1}\left[(f_{\kappa_-}g_{\kappa_+}-g_{\kappa_-}f_{\kappa_+})+\frac{\kappa_+-\kappa_-}{L+1}(f_{\kappa_-}g_{\kappa_+}+g_{\kappa_-}f_{\kappa_+})\right]\right\}r^2dr\ , \tag{23}$$

and $S_{l_1,l_2,L}=\frac{1}{2}[1+(-1)^{l_1+l_2+L}]$ enforces the electric or magnetic multipole selection rules. The electric radial integrals contain j_{L-1} and j_{L+1}, which are somewhat inconvenient to manipulate in the matrix technique used by us to evaluate the radial integrals. We eliminate the j_{L+1} term by carrying out a gauge transformation to the so-called "least singular" gauge. We do this by choosing a gauge function S_λ in

$$\mathbf{A}'_\lambda(\mathbf{r},t)=\mathbf{A}_\lambda(\mathbf{r},t)+\nabla S_\lambda(\mathbf{r},t)\ ,$$
$$\phi'_\lambda(\mathbf{r},t)=\phi_\lambda(\mathbf{r},t)-\frac{\partial S_\lambda}{\partial t}(\mathbf{r},t)\ , \tag{24}$$

to be given by

$$S_\lambda(\mathbf{r},t)=e^{-i\omega t}\sum_L S^\lambda_L(\omega r)Y^\lambda_L(\hat{\mathbf{r}})\ , \tag{25}$$

where

$$S^\lambda_L(\omega r)=\frac{\sqrt{2\pi}i^{L+1}}{\omega}\left[\frac{L(2L+1)}{L+1}\right]^{1/2}j_L(\omega r)\ . \tag{26}$$

The magnetic radial integral $I^{(m)}$ is not affected by the gauge transformation, but the electric radial integral in the least singular gauge becomes

$$I^{(e)}=-\left[\frac{L}{L+1}\right]^{1/2}\int_0^\infty\left\{j_{L-1}\left[(f_{\kappa_-}g_{\kappa_+}-g_{\kappa_-}f_{\kappa_+})-\frac{\kappa_+-\kappa_-}{L}(f_{\kappa_-}g_{\kappa_+}+g_{\kappa_-}f_{\kappa_+})\right]-j_L(f_{\kappa_-}f_{\kappa_+}+g_{\kappa_-}g_{\kappa_+})\right\}r^2dr\ . \tag{27}$$

The fully differential cross section for pair production is

$$\frac{d^3\sigma}{dE_+d\Omega_-d\Omega_+}=\sum\frac{\pi}{I}|V_{f,i}|^2\left[\frac{dn}{dE_-}\right]\left[\frac{dn}{dE_+}\right]\frac{1}{d\Omega_-}\frac{1}{d\Omega_+}\ , \tag{28}$$

where the initial photon flux $I=1/\mathcal{V}$, and the densities of the final states are given as

$$\frac{dn}{dE_-}=\frac{\mathcal{V}p_-E_-}{(2\pi)^3}d\Omega_-\ ,$$
$$\frac{dn}{dE_+}=\frac{\mathcal{V}p_+E_+}{(2\pi)^3}d\Omega_+\ . \tag{29}$$

We integrate Eq. (28) over electron and positron angles by using the orthonormality properties of the spherical harmonics and then summing over spins and polarization to obtain

$$\frac{d\sigma}{dE_+}=\sum_{\kappa_+,\kappa_-,L}\left[\frac{d\sigma}{dE_+}\right]_{\kappa_+,\kappa_-,L}\ ,$$

where

$$\left[\frac{d\sigma}{dE_+}\right]_{\kappa_+,\kappa_-,L}=\frac{2e^2(E_-+m)(E_+-m)p_+p_-}{\omega}\times(2j_-+1)(2j_++1)\times|C^{\,j_+\ j_-\ L}_{-1/2\ 1/2\ 0}R(\kappa_+,\kappa_-,L)|^2 . \tag{30}$$

The expression in Eq. (30) has a different form from that used by Overbo *et al.*[9] since we chose a multipole expansion of the total vector potential, while they choose to use the expansion for the scalar factor $e^{i\kappa\cdot r}$ in the vector potential. Our result has the advantage that the radial integrals enter the differential cross section integrated over the directions of the pair as terms in an incoherent sum. Additional details of the above derivation can be found in Ref. 20.

C. Radial integrals

The radial integrals in Eqs. (22) and (27) are linear combinations of the elements of a matrix gamma function (for definition and other useful properties, see Onley[16] and Sud *et al.*[17]) defined as

$$\Gamma(A+1,B)=\int_0^\infty W(A,B:r)dr , \tag{31}$$

where $W(A,B:r)$ is a direct product of U's and is given as

$$W(A,B:r)=U_g\otimes U_-\otimes U_+ . \tag{32}$$

The two dimensional U's satisfy the matrix differential equation

$$\frac{dU_i}{dr}=\left[\frac{A_i}{r}-B_i\right]U_i,\quad i=+,-,g . \tag{33}$$

We obtain, from Eq. (6),

$$A_\pm=\begin{bmatrix}-\kappa_\pm & \alpha Z\\ -\alpha Z & \kappa_\pm\end{bmatrix},\quad B_+=\begin{bmatrix}0 & E_+-m\\ -(E_++m) & 0\end{bmatrix},$$

and (34)

$$B_-=\begin{bmatrix}0 & -(E_-+m)\\ E_-m & 0\end{bmatrix} .$$

The point Coulomb radial functions U_+ and U_- for positron and electron, respectively, are given in terms of the conventional functions f_κ and g_κ in subsection A. We take U_g to be

$$U_g=\begin{bmatrix}j_L(\omega r)\\ j_{L-1}(\omega r)\end{bmatrix} , \tag{35}$$

and the corresponding A_g and B_g matrices are

$$A_g=\begin{bmatrix}-L-1 & 0\\ 0 & L-1\end{bmatrix},\quad B_g=\begin{bmatrix}0 & -\omega\\ \omega & 0\end{bmatrix} . \tag{36}$$

The one-column matrix function W of products of regular functions satisfies a matrix differential equation of the type (33) with the following 8×8 $\mathcal{A}$ and $\mathcal{B}$ matrices,

$$\mathcal{A}=A_g\otimes I_4+I_2\otimes A_-\otimes I_2+I_4\otimes A_+ ,\quad \mathcal{B}=B_g\otimes I_4+I_2\otimes B_-\otimes I_2+I_4\otimes B_+ , \tag{37}$$

where I_n denotes the $n\times n$ unit matrix. Integrals over the one-column matrix W will be referred to as a vector gamma function, and the pair production radial integrals of Eqs. (22) and (27) are simply given in terms of the elements of this vector gamma function by

$$I^{(m)}=\frac{1}{\sqrt{L(L+1)}}(\kappa_++\kappa_-)(\Gamma_2+\Gamma_3) , \tag{38}$$

$$I^{(e)}=\left[\frac{L}{L+1}\right]^{1/2}\left[\Gamma_1+\Gamma_4+\Gamma_6-\Gamma_7+\frac{\kappa_+-\kappa_-}{L}(\Gamma_6+\Gamma_7)\right] . \tag{39}$$

The direct integration of Eq. (31) will lead to each element of this gamma vector being a Lauricella function[24] with variables

$$x=\frac{2\omega}{p_++p_-+\omega} ,\quad y=\frac{2p_-}{p_++p_-+\omega} ,$$

and

$$z=\frac{2p_+}{p_++p_-+\omega} .$$

Since the condition for convergence of the triply infinite Lauricella series is $|x|+|y|+|z|<1$, these elements cannot be calculated by direct summation of the series without resorting to the analytic continuation of the Lauricella functions. We have followed an alternative approach in which the spherical Bessel functions in U_g [Eq. (35)] can be written as the real part of a finite number of terms,

$$j_L(\omega r)=\mathrm{Re}[h_L^{(1)}(\omega r)] , \tag{40}$$

and the spherical Hankel function is given by

$$h_L^1(\omega r)=e^{i\omega r}\sum_{n=1}^{L+1}a_n(L)r^{-n} ,$$

where

$$a_n(L)=\frac{2\Gamma(L+n)i^{n-L-2}}{\Gamma(n)\Gamma(2+L-n)(2\omega)^n} . \tag{41}$$

Furthermore, the lepton radial functions [Eq. (7)] are real, so we can express Eq. (31) as

$$\Gamma(\mathcal{A}+1,\mathcal{B})=\mathrm{Re}\int_0^\infty\begin{bmatrix}h_L^1(\omega r)\\ h_{L-1}(\omega r)\end{bmatrix}\otimes U_-\otimes U_+dr . \tag{42}$$

We define a four-element vector gamma function such that all r dependence of Eq. (42) is included in it, and is

given as

$$\Gamma(A-n,B-i\omega)=\int_0^\infty \frac{e^{i\omega r}}{r^{n+1}}(U_-\otimes U_+)dr\ , \tag{43}$$

where

$$\begin{aligned} A&=A_-\otimes I_2+I_2\otimes A_+\ ,\\ B&=B_-\otimes I_2+I_2\otimes B_+\ . \end{aligned} \tag{44}$$

We can express Eq. (42) by using Eqs. (40) and (43) and the recurrence relation satisfied by the gamma vector,[16,17]

$$A\Gamma(A,B)=B\Gamma(A+1,B)\ , \tag{45}$$

in the following form,

$$\Gamma(\mathcal{A}+1,\mathcal{B})=X\begin{bmatrix}\Gamma(A-L,B-i\omega)\\ \Gamma(A-L+1,B-i\omega)\end{bmatrix} \tag{46}$$

where the 8×8 matrix X is given as

$$X=\begin{bmatrix}X(L) & 0\\ 0 & X(L-1)\end{bmatrix}\ , \tag{47}$$

with

$$X(L)=a_{L+1}(L)I_4+\sum_{n=2}^{L+1}a_{L+2-n}(L)\times\prod_{m=1}^{n-1}[(B-i\omega)^{-1}\times(A-L+m+1)]\ , \tag{48}$$

where successive terms in the matrix product multiply from the left.

As discussed in detail in the Appendix of Ref. 22, the Dirac-Coulomb functions (and the spherical Bessel or Hankel functions) and the radial integrals over them can be conveniently expressed in the so-called standard representation where f_κ and g_κ are real, or in representations where either the A matrices or B matrices are diagonal. These different representations are labeled with the superscripts (S), (A), and (B), respectively, and the various transformations among the different representations are given in Ref. 22. If one examines Eq. (48), it is clear that since the matrix $B-i\omega$ needs to be inverted, working in the B-diagonal representation is most convenient. Thus the eight-element vector gamma function whose elements can be combined to yield the radial integral can finally be written as

$$\Gamma(\mathcal{A}^{(S)}+1,\mathcal{B}^{(S)})=\mathrm{Re}\left[(I_2\otimes C_-^{SB}\otimes C_+^{SB})\times X^{(B)}\begin{bmatrix}\Gamma(A^{(B)}-L,B^{(B)}-i\omega)\\ \Gamma(A^{(B)}-L+1,B^{(B)}-i\omega)\end{bmatrix}\right], \tag{49}$$

where the transformation matrices from the B-diagonal representation to the standard representation are given in Ref. 22 and the superscript (B) means those functions should be evaluated with all matrices in the B-diagonal form.

In the B-diagonal representation, the elements of B in Eq. (48) are $\pm ip_+\pm ip_-$, and when added to $-i\omega$ one sees that $B^{(B)}-i\omega$ is almost singular for extremely relativistic leptons due to the element $i(p_++p_--\omega)$. It is basically this problem which limits the computer program of Overbo *et al.*[9] to photon energies less than about 5 MeV.

The four elements of $\Gamma(A^{(B)}-n,B^{(B)}-i\omega)$ which appear in Eq. (49) can be written in terms of the Appel function[24] $F_2(\alpha,a_1,a_2,b_1,b_2;x,y)$ by explicit substitution of the lepton wave functions and term by term integration. The parameters α,a_1,a_2,b_1,b_2 depend on $\gamma_\pm$ and $\eta_\pm$, while the variables $x=-2ip_+/\Delta$ and $y=-2ip_-/\Delta$, where $\Delta=-i(p_++p_-+\omega)$. The hypergeometric function F_2 is given in terms of a doubly infinite series as

$$F_2(\alpha,a_1,a_2,b_1,b_2;x,y)=\sum_{m,n}\frac{(\alpha)_{m+n}(a_1)_m(a_2)_n}{(b_1)_m(b_2)_n m!n!}x^m y^n\ , \tag{50}$$

and is absolutely convergent for $|x|+|y|<1$. Thus for pair production where $\omega=E_++E_->p_++p_-$,

$$|x|+|y|=\left|\frac{2p_+}{p_++p_-+\omega}\right|+\left|\frac{2p_-}{p_++p_-+\omega}\right|<1\ . \tag{51}$$

As ω increases, p_+ and p_- approach E_+ and E_- (apart from the endpoint region) and $|x|+|y|$ approaches 1, and the evaluation of F_2 becomes problematic on the computer.

As discussed in Refs. 16, 17, and 22, the Dirac-Coulomb wave functions can be expressed as a 2×2 matrix series and the four elements of Γ in Eq. (41) can be obtained by summing a matrix series in the A-diagonal representation. The resulting series has the form

$$\Gamma(A^{(A)}-n,B^{(A)}-i\omega)=\sum_{m=0}^{\infty}\frac{\Gamma(A_{11}^{(A)}-n+m)\mathbf{V}_m}{(-i\omega)^{A_{11}^{(A)}-n+m}}\ , \tag{52}$$

where $\Gamma(A_{11}^{(A)}-n+m)$ is the conventional gamma function, and the elements of $\mathbf{V}_m$ are given by the recurrence relation,

$$\{V_m\}_i=\frac{B_{ij}^{(A)}(V_{m-1})_j}{A_{11}^{(A)}-A_{ii}^{(A)}+m}\ , \tag{53}$$

with $(V_0)_i=(\mathrm{norm})\delta_{i,1}$. This single matrix series is more quickly summed than the doubly infinite series in Eq. (50) since roughly speaking it is a $4\times\infty$ series rather than an $\infty\times\infty$ series. However, the convergence condition for the matrix series and for the Appell series in terms of the kinematic variables p_+, p_-, ω are identical, so that, for larger ω, numerical difficulties prevent using the matrix series directly just as before.

The procedure given above is formulated somewhat differently than the one used by Overbo *et al.*[9] and the radial integrals can be evaluated more quickly on the computer. However, in the final analysis the numerical difficulties which prevented Overbo *et al.*[9] from evaluating higher angular momenta radial integral also show up

in our procedure. The primary source of the difficulty is the near singularity of the $B-i\omega$ matrix. This near singularity can be avoided by evaluating the radial integrals at a nonphysical value of the photon energy ω', and using the fact that the matrix gamma function obeys a first-order matrix partial differential equation[18] in ω'. That is, we evaluate the vector gamma function of Eq. (42) for $\omega' > \omega$, and then use the differential equation to integrate it back to the physical photon energy $\omega = E_+ + E_-$. This procedure leads to two improvements: (1) the sum of variables $|x| + |y|$ in Appell's series becomes smaller since $\omega' > \omega$, and thus the series converges with fewer terms, and (2) the recurrence on powers of r in Eq. (48) works much better since $B-i\omega$ now has elements $\pm ip_+ \pm ip_- - i\omega'$ and is no longer almost singular.

The first order matrix differential equation satisfied by the eight-element vector gamma function of Eq. (42) in the B-diagonal representation is

$$\frac{d\Gamma(\mathcal{A}^{(B)}+1, \mathcal{B}^{(B)})}{d\omega'} = T\Gamma(\mathcal{A}^{(B)}+1, \mathcal{B}^{(B)}) , \tag{54}$$

where

$$T = \frac{1}{\omega'} A_g^{(B)} \otimes I_4 - \frac{1}{\omega'} B_g^{(B)} \otimes I_4 (\mathcal{B}^{(B)})^{-1} (\mathcal{A}^{(B)}+1) . \tag{55}$$

The matrices $A_g^{(B)}$ and $B_g^{(B)}$ are given by

$$A_g^{(B)} = \begin{bmatrix} -1 & L \\ L & -1 \end{bmatrix}$$

and (56)

$$B_g^{(B)} = \begin{bmatrix} -i\omega' & 0 \\ 0 & i\omega \end{bmatrix}$$

while $A_\pm$ and $B_\pm$ in the B-diagonal representation are

$$A_\pm^{(B)} = \begin{bmatrix} i\eta_\pm & \gamma_\pm - i\eta_\pm \\ \gamma_\pm + i\eta_\pm & -i\eta_\pm \end{bmatrix}$$

and (57)

$$B_\pm^{(B)} = \begin{bmatrix} \pm ip_\pm & 0 \\ 0 & \mp ip_\pm \end{bmatrix} .$$

The 8×8 $\mathcal{A}$ and $\mathcal{B}$ matrices are given in terms of these matrices by Eq. (37).

III. CALCULATIONAL DETAILS

We briefly outline the salient features of our procedure for evaluating the pair production cross section in the distorted Born approximation, which we have used to calculate the pair production cross section for 10 and 20 MeV photons on uranium ($Z=92$). To evaluate the radial integrals which appear in Eq. (30), we first evaluate the four-element gamma vector of Eq. (43) for $n=L$ at the nonphysical photon energy ω' in the A-diagonal representation. For photon energies of 10 and 20 MeV, we have chosen ω' to be between 12 and 15 and 24 and 30 MeV, respectively. We transform these four-element vectors to the B-diagonal representation and use Eq. (46) to form the eight-element gamma vector over the spherical Hankel functions h_L and h_{L-1} from which we can extract the spherical Bessel integrals by transforming to the standard representation and taking the real part of the resulting gamma vector as in Eq. (49). This step is necessary before numerically integrating Eq. (54) to obtain the desired integrals at $\omega' = \omega$ since the spherical Neumann parts of the spherical Hankel integrals are significantly larger than the spherical Bessel parts for large photon angular momenta. The recursion relation which forms the basis of Eq. (48) loses precision after about five steps, so we actually calculate $n = L, L-5, \ldots$, and recur to obtain the intermediate values of n.

The eight-element gamma vector with spherical Bessel functions is transformed back to the B-diagonal representation and is numerically integrated by means of Eq. (54) to $\omega' = \omega$. Once again transforming the gamma vector back to the standard representation, we can use its elements to form the electric and magnetic radial integrals given in Eqs. (38) and (39). In both A-diagonal and B-diagonal representations, the A and B matrices are independent of the sign of kappa, so from a given magnitude of κ_+ and κ_- once can form four radial integrals involving $\pm\kappa_+$ and $\pm\kappa_-$ by only repeating the last transformation back to the standard representation which depends on the signs of the kappas.

For given magnitudes κ_+ and κ_-, the allowed photon multipoles L range from $|\kappa_+ - \kappa_-|$ to $|\kappa_+ + \kappa_- - 1|$. Additional computer time can be saved by using a recursion relation on L for the gamma vector[20,22] which is given by

$$\Gamma(\mathcal{A}(L\pm 1)+1, \mathcal{B}) = [(C_L^\pm \otimes I_4)\mathcal{A}^{-1}\mathcal{B} - (D_L^\pm \otimes I_4)] \times \Gamma(\mathcal{A}(L)+1, \mathcal{B}) . \tag{58}$$

This recursion relation follows from the spherical Bessel recursion relation, which can be written as

$$U_g(L\pm 1) = \left[\frac{C_L^\pm}{r} - D_L^\pm \right] U_g(L) , \tag{59}$$

where U_g is defined in Eq. (35) and C_L and D_L are

$$C_L^+ = \begin{bmatrix} (2L+1/\omega & 0 \\ 0 & 0 \end{bmatrix} ,$$

$$C_L^- = \begin{bmatrix} 0 & 0 \\ 0 & (2L-1)/\omega \end{bmatrix} , \tag{60}$$

$$D_L^\pm = \begin{bmatrix} 0 & \pm 1 \\ \mp 1 & 0 \end{bmatrix} .$$

We evaluate the gamma vector for $L_{\min}$ and recur a maximum of eight times; and if needed, recalculate $L_{\min}+9$ and recur again. The recursion works well, but all recursion relations gradually lose precision in the computer. For large L values ($L > 80$), we find it necessary to reduce the number of recursions to five before recalculating.

The procedure outlined above has been used to evaluate the pair production radial integrals for photon multipoles L and kappa values up to 150, and apart from minor modifications in the number of recursions we find no nu-

merical difficulties for photon energies from 5 to 20 MeV and for values of E_+ and E_- at least 0.15 MeV away from the endpoints. Our procedure requires modification if p_+ or p_- become too small.[12] The remaining difficulty in evaluating the differential cross section for pair production is carrying out the sums over angular momenta.

The differential cross section of Eq. (30) can be expressed as

$$\frac{d\sigma}{dE_+}=\sum_{q=1}^{\infty} T_q \ , \tag{61}$$

where $q=|\kappa_1|+|\kappa_-|-1$, and the terms T_q are given by

$$T_q=\sum_{|\kappa_+|,|\kappa_-|}\delta_{q,|\kappa_+|+|\kappa_-|-1} \times\sum_{L=L_{\min}}^{L_{\max}}\sum_{\substack{\mathrm{sgn}\kappa_+\\ \mathrm{sgn}\kappa_-}}\left[\frac{d\sigma}{dE_+}\right]_{\kappa_+,\kappa_-,L} . \tag{62}$$

In Fig. 2 we show T_q as a function of q for $\omega=10$ MeV and three different positron energies. Note that T_q is a smooth function of q, so in general, we only calculate T_q for $q=1$–40, 60, 80, 100, and 150 and use a spline interpolation of $\ln T_q$ to fill in the other points. In particular, note that $\ln T_q$ versus q approaches a straight line for large values of q. Assuming this linear behavior continues permits us to use the slope (a) of the $\ln T_q$ versus q at $q=q_{\max}$ to calculate the remaining contributions. That is,

$$\frac{d\sigma}{dE_+}=\sum_{q=1}^{q_{\max}} T_q+R \ , \tag{63}$$

where the remainder R is given by

$$R=T_{q_{\max}}\frac{e^a}{1-e^a} \ . \tag{64}$$

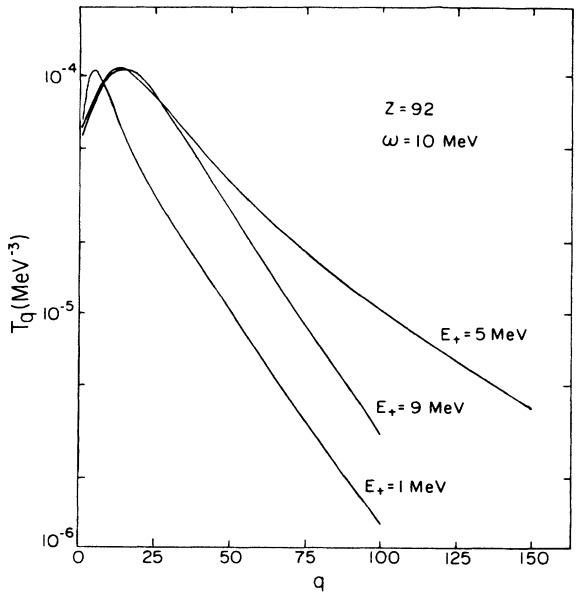

FIG. 2. The terms T_q as a function of q for various positron energies for 10 MeV photons on uranium ($Z=92$).

For $\omega=10$ MeV, the remainder at $q=150$ is less than 2% of the total sum apart from midrange cases where the photon energy is more evenly shared by the positron and electron. There the remainder is less than 4% of the total. For $\omega=20$ MeV, the remaining percentages are larger and amount to 4% for uneven energy splits and 10% for more even energy splits. Of course, if the slope (a) is still varying, this extrapolation leads to errors in our estimate of the remainder. In order to estimate the error in the remainder, we compare $\exp(a)$ at $q=100$ and 150 and take this variation to generate an estimated error in the remainder R. For $\omega=10$ MeV, this estimated uncertainty in R leads to an uncertainty in the differential cross section of less than 0.2%. For the point in the middle of the 10 MeV spectrum, we adopted an alternate procedure. When $E_+=\omega/2$, the differential cross section can only depend on even powers of the charge Z, and we found that T_q for large values of q becomes independent of Z. Thus by adding and subtracting the plane wave cross section σ_{BH} (which we assume is well represented by $Z=1$ in the partial wave expansion method), we can calculate the differential cross section by writing

$$\left[\frac{d\sigma}{dE_+}\right]_{Z=92}=\sum_{q=1}^{q_{\max}}[T_q(92)-T_q(1)]+\sigma_{\mathrm{BH}} \ . \tag{65}$$

To confirm that $Z=1$ for large q reproduces the plane wave result well, we compare T_{150} for E_+ of 6.5 and 3.5 MeV. For the plane wave case, these points are identical. Using $Z=1$ we find $0.350\,28\times10^{-5}$ and $0.350\,47\times10^{-5}$, respectively, which only differ by 0.05%. For $E_+=5$ MeV, T_{150} for $Z=1$ and 92 only differ by 0.2%, so we conclude that the differential cross section evaluated with this method is accurate to within 0.2%. For 10 MeV photons on uranium ($Z=92$) we have calculated $d\sigma/dE_+$ for the values of E_+ shown in Table I by the methods described above, apart from the point at $E_+=9.4849$ MeV, which was obtained from Ref. 12. Our estimate is that

TABLE I. Differential cross sections for pair production from $Z=92$ with 10 MeV photons for different positron energies. The labels DW, SM, and BH corresond to the present calculation, Borie's Sommerfeld-Maue results (Ref. 25), and the plane wave Bethe-Heitler results, respectively.

E_+ (MeV)	$d\sigma_{\mathrm{DW}}/dE_+$ (10^{-3} MeV^{-3})	$d\sigma_{\mathrm{SM}}/dE_+$ (10^{-3} MeV^{-3})	$d\sigma_{\mathrm{BH}}/dE_+$ (10^{-3} MeV^{-3})
0.75	1.005		2.298
1.00	2.350	1.396	3.337
1.40	3.426		4.383
1.75	4.120	3.246	4.952
2.10	4.493		5.326
2.50	4.761	4.077	5.599
3.50	5.041	4.535	5.895
5.00	5.162	4.724	5.967
6.50	5.197	4.686	5.895
7.50	5.140	4.422	5.599
8.25	4.894	3.897	4.952
9.00	4.098	2.762	3.337
9.25	3.567	2.160	2.298
9.4849	2.707		0.1245

these differential cross sections are accurate to ±0.25%.

We have carried out similar calculations for 20 MeV photons on uranium ($Z=92$), but as mentioned above the sum over q has not converged as well at this higher photon energy. To improve our results when E_+ is well away from the endpoints, we make use of the Sommerfeld-Maue (SM) approximation by writing

$$\frac{d\sigma}{dE_+}=\sum_{q=1}^{q_{\max}}[T_q(\mathrm{DW})-T_q(\mathrm{SM})]+\left[\frac{d\sigma}{dE_+}\right]_{\mathrm{SM}}, \tag{66}$$

where $T_q(\mathrm{SM})$ is defined in terms of $(d\sigma/dE_+)^{\mathrm{SM}}_{\kappa_+,\kappa_-,L}$ just as $T_q(\mathrm{DW})$ is defined in Eq. (62), and the same formalism is used for the radial integrals, except that $\gamma\rightarrow\kappa$ everywhere. The Sommerfeld-Maue cross section $(d\sigma/dE_+)_{\mathrm{SM}}$ is a numerical integration over lepton angles of the Sommerfeld-Maue result obtained from Borie.[25] For uneven energy splits we sum the DWBA series to $q_{\max}=150$ and use the linear extrapolation of $\ln T_q$ as in the 10 MeV case to add in the remainder since the Sommerfeld-Maue approximation breaks down when one of the lepton energies is too small. In Table II we give the differential cross sections for photon energy $\omega=20$ MeV on uranium for a number of positron energies. The cross sections with an asterisk were evaluated with the help of the SM results as shown in Eq. (66).

IV. RESULTS AND CONCLUSIONS

In Tables I and II we present the results of our calculations of the differential cross section for photon energies of 10 and 20 MeV for uranium ($Z=92$) for different positron energies. We also compare our results with the PW result of Bethe-Heitler[7] and results from the Sommerfeld-Maue approximation[25,26] obtained by numerical integration over the lepton angles without resorting to the high energy approximation. In order to obtain the total pair production cross section, we use a spline interpolation program which suppresses waves in the fitted curve[27] to obtain the results at 10 and 20 MeV shown in Figs. 3 and 4. These curves allow us to calculate the total DWBA cross sections by Gaussian integration that are shown in Table III along with the predictions by Overbo,[14] Maximon and Gimm,[15] Davies-Bethe-Maximon,[13] the Sommerfeld-Maue approximation,[24] and the experimental results of Sherman *et al.*[3] modified by screening and radiative corrections.

Note that the total cross section predictions by the two different interpolation formulas differ from each other by 0.68% of the Bethe-Heitler result at 10 MeV and 0.99% of the Bethe-Heitler result at 20 MeV. Since neither of the interpolating formulas can be derived from theory, it is not surprising that they differ from each other and from our results.

In Fig. 5 we show the ratios of the total cross section to the Bethe-Heitler result for the two bridging formulas and the high energy DBM result as a function of photon energy for $Z=92$. The ratios from our calculated values lie between the two bridging formulas, but are slightly closer to the Maximon-Gimm curve. In order to compare our calculated results with the observations of Sherman *et al.*,[5] we have divided σ_{obs} by the Mork-Olsen radiative correction f_{rad} and the screening correction $1-R$ interpolated from Hubbell *et al.*[6] We refer to this result as the "experimental" cross section $\sigma_{\text{"expt"}}$, and our DWBA results differ considerably from these values. The "experi-

TABLE II. Differential cross sections for pair production from $Z=92$ with 20 MeV photons for different positron energies. The labels DW, SM, and BH correspond to the present calculation, Borie's Sommerfeld-Maue results (Ref. 25), and the plane wave Bethe-Heitler results, respectively. The values with an asterisk were calculated using the partial wave decomposition of the Sommerfeld-Maue approximation.

E_+ (MeV)	$d\sigma_{\mathrm{DW}}/dE_+$ (10^{-3} MeV^{-3})	$d\sigma_{\mathrm{SM}}/dE_+$ (10^{-3} MeV^{-3})	$d\sigma_{\mathrm{BH}}/dE_+$ (10^{-3} MeV^{-3})
0.60	0.0248		
0.65	0.0934		
1.00	1.251	0.794	1.864
1.50	2.061	1.642	2.659
2.50	2.828*	2.586	3.494
5.00	3.467*	3.359	4.111
7.50	3.563*	3.488	4.164
12.50	3.606*	3.511	4.164
15.00	3.586*	3.427	4.111
17.50	3.185*	2.832	3.494
19.00	2.314	1.574	1.864
19.15	2.117	1.360	1.526
19.35	1.552	1.039	0.931

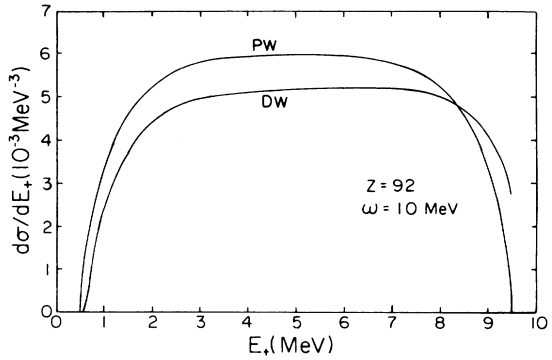

FIG. 3. The differential cross section for pair production of 10 MeV photons on $Z=92$ as a function of positron energy. For the distorted wave (DW) results, the points given in Table I were interpolated using a spline interpolation program (Ref. 27). The curve labeled PW is the Bethe-Heitler result.

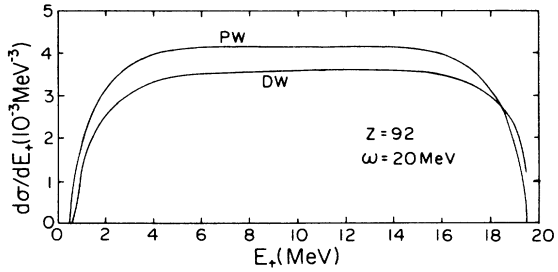

FIG. 4. Same as Fig. 3, except the photon energy is 20 MeV.

TABLE III. Total pair production cross sections for $Z=92$ and photon energies of 10 and 20 MeV. The subscripts DW, "expt," MG, Ov, SM, and BH correspond to the present calculation, the experimental results of Sherman *et al.* (Ref. 3), as divided by f_{rad} and $1-R$, the Maximon-Gimm interpolation (Ref. 15), the Overbo interpolation (Ref. 14), the Sommerfeld-Maue results of Borie (Ref. 25), and the plane wave Bethe-Heitler results. All the cross sections are in 10^{-2} MeV^{-2}.

Photon energy (MeV)	σ_{DW}	$\sigma_{\text{"expt"}}$	σ_{MG}	σ_{Ov}	σ_{SM}	σ_{BH}
10	4.085	4.238±0.024	4.073	4.101	3.463	4.593
20	6.128	6.193±0.018	6.091	6.162	5.757	7.076

mental" values are higher by 3.7% at 10 MeV and 1.1% at 20 MeV than our theoretical results. As discussed in the preceding section, we estimate the maximum error in our 10 MeV differential cross sections to be 0.25% and believe that our errors at 20 MeV are comparable. However, due to the use of the partial wave expansion of the Sommerfeld-Maue approximation at 20 MeV which includes a second-order term that is neglected in the analytic Sommerfeld-Maue approximation, we cannot be as sure in our error estimate at 20 MeV.[20] Furthermore, the spline interpolation used to generate the total cross section could introduce additional errors. To examine this source of error, we carried out the interpolation with one or more calculated points omitted and found very small deviations in the interpolated value of the point omitted and the total cross section if we forced the spline interpolation to be quite smooth. Our best estimate is that our total cross section results have a maximum uncertainty of 0.5%, and thus are in disagreement with the "experimental" results.

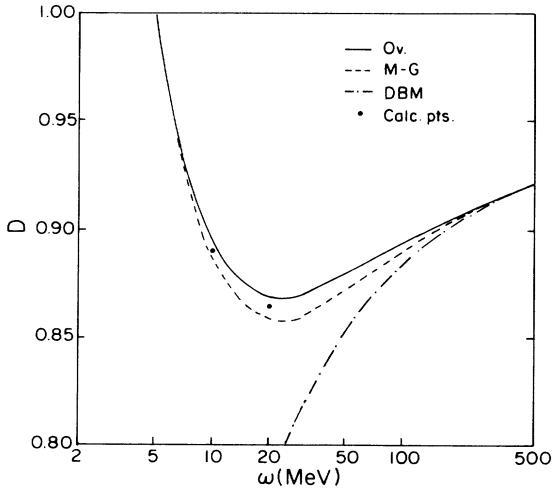

FIG. 5. D, the ratio of the total cross section to the Bethe-Heitler result, as a function of photon energy for $Z=92$, is shown for the interpolation formulas of Overbo (Ref. 14) and Maximon and Gimm (Ref. 15) and for the high energy Sommerfeld-Maue approximation of Davies, Bethe, and Maximon (Ref. 13). The two points are the results of the present calculation.

In order to explore the possible reasons for this discrepancy between the "experimental" and theoretical results, it is worthwhile to examine the technique used by Sherman *et al.*[3] to extract the pair production cross sections. The experimental pair production cross sections have been obtained from the measured total photon absorption cross sections by subtracting the theoretical atomic absorption cross sections and the photonuclear absorption cross section. The atomic cross sections have been obtained by interpolation from the tables of Refs. 5 and 6 which claim an accuracy of better than 0.2%, and the photonuclear cross section has been assumed to be given by the experimental photoneutron cross section. In order to compare our DWBA theoretical results with the experimental pair production cross section, one needs to take into account the correction due to the screening of the point Coulomb field by atomic electrons. Davis, Bethe, and Maximon[13] have shown in the high energy limit that the corrections for screening and for Coulomb distortion are independent since the screening is mainly related to the small momentum region while the Coulomb corrections arise due to close encounters which involve large momentum transfer. It is not obvious that this separation is valid in the intermediate energy range or in the intermediate momentum transfer range, particularly to the degree needed in the present comparison of theory and experiment. We see need for a full DWBA model calculation with some simple atomic potential to investigate the question of the separability of the Coulomb distortion and screening effects.

In addition, the screening corrections used have been calculated in the form factor approximation (see Hubbell *et al.*[6] for details) in the Born approximation, but the form factor approach does not predict the screening effects correctly in the low energy region.[10] The discrepancy observed between the theoretical and "experimental" results strongly suggest that the screening effects[6] have not been properly calculated in this energy region and need further investigation.

In conclusion, we point out that we have demonstrated that a full DWBA calculation of pair production from a point charge in the intermediate energy region is feasible using the improved techniques of evaluating the Dirac-Coulomb radial integrals. Based on work involving similar integrals in bremsstrahlung,[22] we should be able to include the effect of finite nuclear size which may also be one of the reasons for the discrepancy between theory and

"experiment." However, nuclear size effects would certainly be larger at 20 MeV than at 10 MeV, while the discrepancy is larger at 10 MeV. A DWBA calculation which properly includes screening appears to be very difficult. However, as mentioned above, a model calculation with a simplified atomic charge distribution may be used to investigate the separability of screening and Coulomb distortion. Finally, our calculation should be used for a number of other energies between 5 and 30 MeV and for other nuclei to modify and improve existing interpolating formulas for Coulomb distortion.

ACKNOWLEDGMENTS

One of us (L.E.W.) wants to thank Professor B. Ziegler of the Max-Planck-Insitut in Mainz for arranging for Cray computer time in Garching and W. Turnov of Mainz University for providing the spline interpolating computer program. We also thank E. Borie for calculating the differential pair production cross sections using the Furry-Sommerfeld-Maue wave functions for us. This work was supported in part by U.S. Department of Energy Grant DE-AC02-79ER10397-07.

---

*Present address: Department of Physics, University of Jodhpur, Jodhpur 342001, India.

[1]J. Ahrens, H. Borchert, K. H. Czock, H. B. Eppler, H. Gimm, H. Gundrum, M. Kroning, P. Riehn, G. Sita Ram, A. Ziegler, and B. Ziegler, Nucl. Phys. **A251**, 479 (1975).

[2]N. K. Sherman and G. M. Ewart, Can. J. Phys. **59**, 914 (1981); Phys. Rev. C **27**, 1011 (1983).

[3]N. K. Sherman, W. F. Davidson, A. Nowak, M. Kosaki, J. Roy, W. Delbianco, and G. Kojrys, Phys. Rev. Lett. **54**, 1649 (1985).

[4]G. M. Gurevich, L. E. Lazareva, V. M. Mazur, S. Yu. Meskulov, and G. V. Soldukhov, Nucl. Phys. **A388**, 97 (1978).

[5]H. Gimm and J. H. Hubbell, Natl. Bur. Stand. (U.S.) Tech. Note No. 968 (1978).

[6]J. H. Hubbell, H. A. Gimm, and I. Overbo, J. Phys. Chem. Ref. Data **9**, 1023 (1980).

[7]H. A. Bethe and W. Heitler, Proc. R. Soc. London, Ser. A **146**, 83 (1934).

[8]J. C. Jaeger and H. R. Hulme, Proc. R. Soc. London **153**, 443 (1936).

[9]I. Overbo, K. J. Mork, and H. A. Olsen, Phys. Rev. **5**, 1978 (1968); A **8**, 668 (1973).

[10]H. K. Tseng and R. H. Pratt, Phys. Rev. A **4**, 1935 (1971).

[11]J. J. Dugne and J. Proriol, Phys. Rev. A **13**, 1793 (1976).

[12]K. K. Sud and D. K. Sharma, Phys. Rev. A **30**, 2311 (1984).

[13]H. Davies, H. A. Bethe, and L. C. Maximon, Phys. Rev. **93**, 788 (1954).

[14]I. Overbo, Phys. Lett. **71B**, 412 (1977).

[15]L. C. Maximon and H. A. Gimm, Natl. Bur. Stand. (U.S.) Internal Report 78-1456, 1978.

[16]D. S. Onley, in *Nuclear Structure Studies Using Electron Scattering and Photoreaction* (Tohoku University, Sendai, Japan, 1972).

[17]K. K. Sud, L. E. Wright, and D. S. Onley, J. Math. Phys. **17**, 2175 (1976).

[18]L. E. Wright, D. S. Onley, and C. W. Soto Vargas, J. Phys. A **10**, L53 (1977).

[19]K. K. Sud, D. K. Sharma, and A. R. Sud, Phys. Rev. A **20**, 2029 (1979).

[20]D. W. Kosik, Ph.D. dissertation, Ohio University, 1980.

[21]L. E. Wright and Indu Talwar, J. Phys. A **19**, 1567 (1986).

[22]Indu Talwar, L. E. Wright, D. S. Onley, and C. W. Soto Vargas, Phys. Rev. C **35**, 510 (1987).

[23]W. R. Johnson and R. T. Deck, J. Math. Phys. **3**, 319 (1962).

[24]P. Appell and J. Kampe de Feriet, *Fonctins Hypergeometriques et Hyperspheriques* (Gauthier-Villars, Paris, 1926).

[25]E. Borie, Z. Phys. A **302**, 219 (1981), and private communication.

[26]J. Fink and R. H. Pratt, Phys. Rev. A **7**, 392 (1973).

[27]V. Tornow, Comput. Phys. Commun. **28**, 61 (1982).